Journal of Catalysis 281 (2011) 137–146

Contents lists available at ScienceDirect

Journal of Catalysis

journal homepage: www.elsevier.com/locate/jcat

Size- and shape-controlled palladium nanoparticles in a fluorometric Tsuji–Trost reaction

Yuwei Yang [a], Larry D. Unsworth [a,b], Natalia Semagina [a,*]

[a] Department of Chemical and Materials Engineering, University of Alberta, Edmonton, Canada T6G 2V4
[b] National Research Council, National Institute of Nanotechnology, Edmonton, Canada T6G 2M9

ARTICLE INFO

Article history:
Received 8 January 2011
Revised 14 April 2011
Accepted 17 April 2011
Available online 17 May 2011

Keywords:
Allylic substitution
Leaching
Palladium nanoparticles
Size control
Oxidative addition
Tsuji–Trost
Atomic dissolution
Ostwald ripening
Fluorometry

ABSTRACT

Palladium nanospheres of 2.4 and 3.8 nm diameter and nanocubes of 18 nm rib length were used to catalyze a fluorometric Tsuji–Trost reaction for the transformation of a phenyl allyl ether to a fluorescent phenol in the presence of triphenylphosphine, which was pivotal to the catalytic activity. Turnover frequencies calculated per defect atoms were found similar for all nanoparticles, indicating that these atoms are the active sites. However, kinetic studies combined with Pd leaching and transmission electron microscopy analyses in the presence of various reaction components showed Pd leaching *via* oxidative addition of a reactant, followed by nanoparticle growth depending on the PPh_3 concentration. The formation of largest particles was found for the fastest reaction with PPh_3/Pd molar ratio of 4, in the range from 0 to 9. This study shows the validity of the atomic dissolution mechanism in the reaction of interest.

1. Introduction

Nanoparticle-catalyzed reactions for constructing C–C, C–N, and C–O bonds, which are traditionally carried out with homogeneous catalysts, have attracted considerable attention in the past decade, and were the subject of recent multiple reviews with detailed discussions on the ways to assess the reaction mechanisms and identify true catalytic species [1–12]. Most of the studies have been devoted to Pd-catalyzed Heck [9,10,13–19], Sonogashira [20–24], and Suzuki [2,25–31] cross-coupling reactions. Although a consensus has been reached on the possibility of using metal nanoparticles as catalysts, the debate persists as to whether the catalysis is intrinsically heterogeneous and occurs *via* reactant adsorption on the surface of nanoparticles or whether atoms leaching from the nanoparticles promote the traditional homogeneous path. For example, Suzuki reaction was suggested to proceed both *via* the atom-leaching mechanism [25,26,28,29] and heterogeneously [27,31], probably, on the surface of metal nanoparticles with defect (edge and corner) atoms as active sites [27]. Controversial data were obtained for the Heck reaction; defect sites on metal nanoparticles were shown to be active sites for the heterogeneously catalyzed reaction [13], while other works showed that nanoparticles serve only as a reservoir for active molecular species [14–17]. In Sonogashira reactions, apart from a heterogeneous mechanism [22], atoms were proposed to leach from defect sites on the Pd cluster, forming active homogeneous species, which recluster after a catalytic cycle [20]. Atomic dissolution due to the oxidative addition of a reactant was suggested as well [21]. One of the premier indicators of the leaching mechanism is the change in size and/or shape of metal nanoparticles during catalysis [26]. If atom leaching occurs, the nanoparticle can either grow larger due to Ostwald ripening, when atoms detach from smaller clusters and reattach to large ones [26], or become smaller, when the detached atoms recluster in new nanoparticles [20]. A particular attention should be drawn to active traces of palladium, either leached during a reaction or present in the reaction components, as discussed in detail in [1].

The nanoparticle-catalyzed allylic substitution, also known as a Tsuji–Trost reaction (Fig. 1a), has been addressed in very few works [4,32–36]. Pd/C [32] was shown to catalyze allylic substitution in water, and no Pd leaching to the solution was found *via* inductively coupled plasma mass spectrometry. However, the nanoparticle sizes before and after the reactions were not monitored. For another Tsuji–Trost reaction, Pd/C was found inactive, while Pd/montmorillonite allowed more than 90% product yield

* Corresponding author. Address: Department of Chemical and Materials Engineering, University of Alberta, 9107-116 St., Edmonton, AB, Canada T6G 2V4. Fax: +1 780 492 2281.
E-mail address: semagina@ualberta.ca (N. Semagina).

0021-9517/$ - see front matter © 2011 Elsevier Inc. All rights reserved.
doi:10.1016/j.jcat.2011.04.009

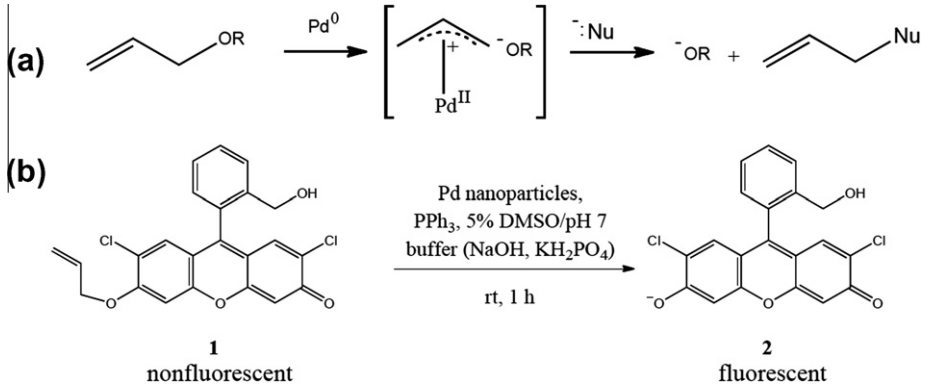

Fig. 1. (a) Tsuji–Trost reaction; (b) schematic of the method for fluorometric detection of palladium: phenyl allyl ether ***1*** is a non-fluorescent sensor, which develops fluorescence upon converting to phenol ***2*** *via* Tsuji–Trost catalysis [35]. The reaction conditions correspond to the current work.

[33]. The presence of triphenylphosphine was shown to be pivotal to the activity of some heterogeneous Pd catalysts, including Pd/C [37]. Pd nanoparticles stabilized by xylofuranoside diphosphite were active in enantioselective allylic alkylation [34], but the reported transmission electron microscopy (TEM) images could not verify whether sub-nanometer changes in nanoparticle size occurred. Studies of Pd nanoparticles in allylic alkylation of different substrates revealed that the metal activity and reaction mechanism depend strongly on the nanoparticle-stabilizing ligands, as well as on the reaction substrate used [38]. Recently, Koide et al. reported an elegant study on fluorometric Pd detection *via* Tsuji–Trost reaction, which yielded a fluorescent phenol ***2*** from a non-fluorescent sensor, phenyl allyl ether ***1*** (Fig. 1b) [35,36]. The reaction was catalyzed by a homogeneous catalyst $Pd(PPh_3)_4$; palladium in catalytic converters and Pd black were detected as well, but no detailed studies on the heterogeneous systems were performed.

In this work, to the best of our knowledge, we are first to report a fluorometric Tsuji–Trost reaction catalyzed by Pd nanoparticles of different shapes and sizes. The selected reaction is the one reported by Koide for the transformation of phenyl allyl ether ***1*** to phenol ***2*** (Fig. 1b) [35,36] due to its prospective application in the simple Pd detection using a fluorometer or a handheld UV lamp. The objective of this study is to establish whether the reaction is heterogeneously catalyzed by surface Pd atoms or proceeds through atomic leaching in the absence of other active traces of palladium in the reaction mixture. The selected particles are nanospheres of 2.4 and 3.8 nm diameter, as well as nanocubes with 18 nm rib length. The range of sizes and shapes covers dispersions varying from 5% to 40% with 13% to 0.1% of defect (edge and vertex) atoms relative to total atoms in the nanoparticles. As the nanoparticles are well defined and there are no Pd impurities in the reaction mixture, correlation of the catalytic activity with surface statistics can be performed, which was found useful in active site determination [13,27,39,40].

2. Materials and methods

2.1. Materials

The list of materials used for phenyl allyl ether ***1*** synthesis is provided in the Supplementary Content. For the nanoparticle preparation and Pd-catalyzed reactions, the following materials were used as received: tetrakis(triphenylphosphine)palladium(0) (99%, Sigma–Aldrich), bis(triphenylphosphine)palladium(II) dichloride ($\geqslant$ 99.9%, Sigma–Aldrich), triphenylphosphine (99%, Sigma–Aldrich), dimethyl sulfoxide (DMSO, ACS spectrophotometric grade, $\geqslant$99.9%, Sigma–Aldrich), buffer solution pH 7.0 at 20 °C (0.12% NaOH, 0.68% KH_2PO_4 in water, Sigma–Aldrich), palladium(II) chloride (solution, 5% w/v in dilute HCl, Acros Organics), poly(*N*-vinyl-2-pyrrolidone) (PVP, average molecular weight 40,000, Sigma–Aldrich), hexadecyltrimethylammonium bromide (CTAB, powder, $\geqslant$98.0%, Sigma–Aldrich), and L-ascorbic acid (puriss. p.a., $\geqslant$99.0%, Sigma–Aldrich). Milli-Q water was used throughout the study. Alumina (activated, weakly acidic γ-Al_2O_3, 150 mesh, 5.8 nm pore size, surface area of 155 m^2/g, Sigma–Aldrich) was calcined at 200 °C prior to nanoparticle deposition.

2.2. Synthesis of phenyl allyl ether ***1*** and phenol ***2***

Phenyl allyl ether ***1*** (6-allyloxy-2,7-dichloro-9-[2-(hydroxymethyl)phenyl] xanthen-3-one) was synthesized from commercially available 2′,7′-dichlorofluorescein and purified according to known procedures [35,41]. Phenol ***2*** (2,7-dichloro-6-hydroxy-9-[2-(hydroxymethyl)phenyl]xanthen-3-one) was prepared and purified for the purpose of fluorometer calibration, using homogeneous Pd catalyst as described elsewhere [35]. The procedure details and ^{1}H NMR data for the synthesized compounds are provided in the Supplementary Content file.

2.3. Synthesis and characterization of Pd catalysts

2.3.1. Pd spheres

Size-controlled Pd nanospheres were prepared according to a known method using poly(*N*-vinyl-2-pyrrolidone) (PVP) as a stabilizer [42]. A larger particle size was obtained *via* stepwise growth reaction [43].

For the preparation of 2.4-nm particles, 50 ml of 2.0 mM H_2PdCl_4 solution was mixed with 0.222 g PVP solution in 117 mL of ethanol/water (2/3 vol.), resulting in molar ratio of PVP monomeric unit to Pd of 20. The mixture was heated under reflux for 3 h in air and then cooled to room temperature. Fifty milliliters of the resulting Pd-PVP nanoparticle colloids was set aside as seeds for stepwise growth to prepare larger particles.

For the preparation of larger nanoparticles, a 0.6 mM H_2PdCl_4 solution was prepared in ethanol/water (2/3 vol.). The seed solution from the previous step (0.6 mM, 50 ml) was mixed with 50 ml of 0.6 mM H_2PdCl_4, and the mixture was heated under reflux for 3 h in air to produce the second-step nanoparticles. The 3.8-nm nanoparticles were prepared in a similar way by using the second step's nanoparticles as seeds.

The obtained colloidal dispersions were dialyzed against water using cellulose membrane with molecular weight cutoff of 3500 to remove unreduced Pd^{2+} and synthesis by-products.

2.3.2. Pd cubes

Pd nanocubes were prepared according to the method reported by Xu, using hexadecyltrimethylammonium bromide (CTAB) as a stabilizer [44]. A 12.5 mM CTAB solution (100 ml) and 10 mM H_2PdCl_4 solution (5 ml) were mixed and heated at 95 °C for 5 min, followed by the addition of 0.8 ml of 100 mM ascorbic acid solution. The mixture was heated at 95–100 °C for 30 min and then cooled. The colloidal dispersion was dialyzed against water.

2.3.3. Preparation of supported catalysts

As industrial heterogeneous catalysts typically consist of a powdered or granulated support with deposited metal nanoparticles, the synthesized Pd spheres and cubes were deposited on γ-Al_2O_3. Dialyzed Pd colloids were stirred with the support and acetone (5-fold volumetric excess as compared to the Pd colloidal dispersion) for 1 h. The clear top solution was decanted, and the remaining slurry was air-dried overnight to give 0.3 wt.% Pd/Al_2O_3.

For comparison purposes, 0.3 wt.% $PdCl_2/Al_2O_3$ catalyst was prepared *via* incipient wetness impregnation of alumina with H_2PdCl_4 solution.

2.3.4. Characterization

TEM images were recorded at 200 kV using a JEOL 2100 transmission electron microscope. Samples were prepared by placing a drop of the colloidal dispersions of nanoparticles onto a carbon-coated copper grid, followed by evaporating the solvent at room temperature. Sizes of over 150 particles were examined per grid. For the leaching studies, the reaction mixtures after catalytic reactions were centrifuged; the supernatant was taken for TEM sample preparation to examine the size of the leached nanoparticles. To observe the changes in the nanoparticles remaining on the support, the recovered catalyst was suspended in ethanol and ultrasonically treated for 2 min to detach nanoparticles from the alumina support; the top clear solution was taken for TEM analysis. The size distribution histograms are presented for two independently prepared batches of each catalyst. The data are reported as average with one standard deviation.

Pd loading on the fresh and used catalysts was determined *via* atomic absorption spectroscopy (AAS) using a Varian 220 FS instrument after the metal dissolution in hot nitric acid. X-ray photoelectron spectroscopy (XPS) was performed with a Kratos Axis 165 X-ray photoelectron spectrometer.

2.4. Catalytic reactions

Catalytic reactions were performed in 4 ml of 5% DMSO/pH 7 buffer solution with varying concentrations of PPh_3 (from 0 to 500 μM), 12.5 μM of the phenyl allyl ether ***1***, and a catalyst (from 0 to 560 μM Pd) under stirring at room temperature in air atmosphere. Most of the experiments were performed at 0.22 mol/mol substrate-to-Pd ratio (unless indicated otherwise); this ratio is not the ratio of the substrate to the catalytically active Pd, but to the total Pd. As this work will show, only a part of the introduced Pd is catalytically active, such as leached atoms from low-coordinated sites from the smallest particles present in the Pd sample. The exact quantity of substrate to catalytically active Pd cannot be estimated as the observed kinetics does not allow separating kinetics of the atomic leaching, Ostwald ripening, and the catalytic reaction. As a confirmation of the catalytic role of Pd in this particular reaction, Koide performed this reaction with only 0.5 mol% $Pd(PPh_3)_4$ [35] but when Pd black was tested (which has particles even larger than our tested nanoparticles with fewer low-coordinated sites), the substrate-to-Pd molar ratio decreased to >0.005 [36], which is again an indirect indication that not all atoms are active.

After a defined period of time, the reaction mixture was centrifuged, and the clear supernatant was used to measure the fluorescence intensity with a Cary Eclipse Fluorescence Spectrophotometer, Varian. Some reactions were quenched by the addition of N-acetylcysteine in DMSO (12.5 M equivalent of Pd), which is a known poison for Pd catalysts, but no differences in the fluorescent intensities were observed (less than 1%) as compared to the solutions without the poison addition. Thus, the experiments were performed without the poison. The spectrophotometer was calibrated using the purified phenol ***2*** in 5% DMSO/pH 7 buffer at different PPh_3 concentrations, which affected fluorescence. Phenol ***2*** exhibited maximum fluorescence at 525 nm. New test tubes were used for each catalytic reaction to avoid possible contamination with Pd traces. None of the reactions, even those catalyzed by Pd^{2+}, showed shift of the fluorescence peak, indicating that aromatic Claisen rearrangement did not occur [45]. The reactions were performed at least three times to ensure reproducibility, and the data are reported as an average with one standard deviation.

3. Results and discussion

3.1. Effect of the nanoparticle size and shape

TEM images and particle size distribution histograms for synthesized Pd nanospheres and cubes (Fig. 2) correlate with expected values [42–44]. Pd nanospheres of 2.4 ± 0.7 and 3.8 ± 0.5 nm have been characterized previously and were assigned an f.c.c. cuboctahedral structure [42,43]. The assumption is in line with the theoretical prediction of Pd nanoparticles having cuboctahedral shape for the number of atoms larger than 561 [46,47], which corresponds to the 2.4-nm Pd particle [42,43]. The Pd cubes were shown to have an f.c.c. structure as well [39]. The "near-cube" length and width are in the range of 17 ± 2 and 19 ± 2 nm, respectively; thus, due to the low aspect ratio, the cubes were assumed to have equal ribs with the length of 18 ± 2 nm.

The nanoparticles supported on γ-Al_2O_3 were tested in the reaction presented in Fig. 1b. To ensure that the observed reaction rates reflect the intrinsic kinetics, the absence of liquid–solid external and internal mass transfer limitations was verified *via* the Madon–Boudart test [48]. The most active particles were chosen as faster reactions are more prone to mass transfer limitations. Three catalysts with 0.15, 0.3, and 0.5 wt.% loading of Pd nanoparticles of 2.4 nm size displayed the same activity at 15% conversion per Pd quantity in the reaction (within 15% experimental error, at 500 μM PPh_3), which ensured that the reactions proceeded in the kinetic regime.

The fluorescence spectra recorded at different reaction times exhibited maximum emission peak at 525 nm, which is in line with results reported by Koide [35], and this observation was attributed to the product formation. Two control experiments, with no catalyst present and with only alumina (2500 ppm), revealed negligible fluorescence intensity (less than 10 a.u. as compared to hundreds a.u. in the catalytic experiments), indicating that the fluorescence observed in the catalytic experiments is due to Pd presence in the catalyst, with negligible activity of Pd traces (if any), which are known to contribute to the observed activity [1]. Fig. 3 shows an example of the kinetic curve obtained for the 2.4-nm spheres at 500 μM PPh_3. The fluorometer calibration was performed for product concentrations from 0 to 12.5 μM, which corresponds to 100% conversion, and allowed for the conversion of the observed intensities to the product concentrations. The plateau in Fig. 3 was reached at 35% conversion. As will be discussed in Section 3.2, the maximum conversion value depends on the PPh_3 concentration and attained 100% when 200 μM PPh_3 was used, indicating

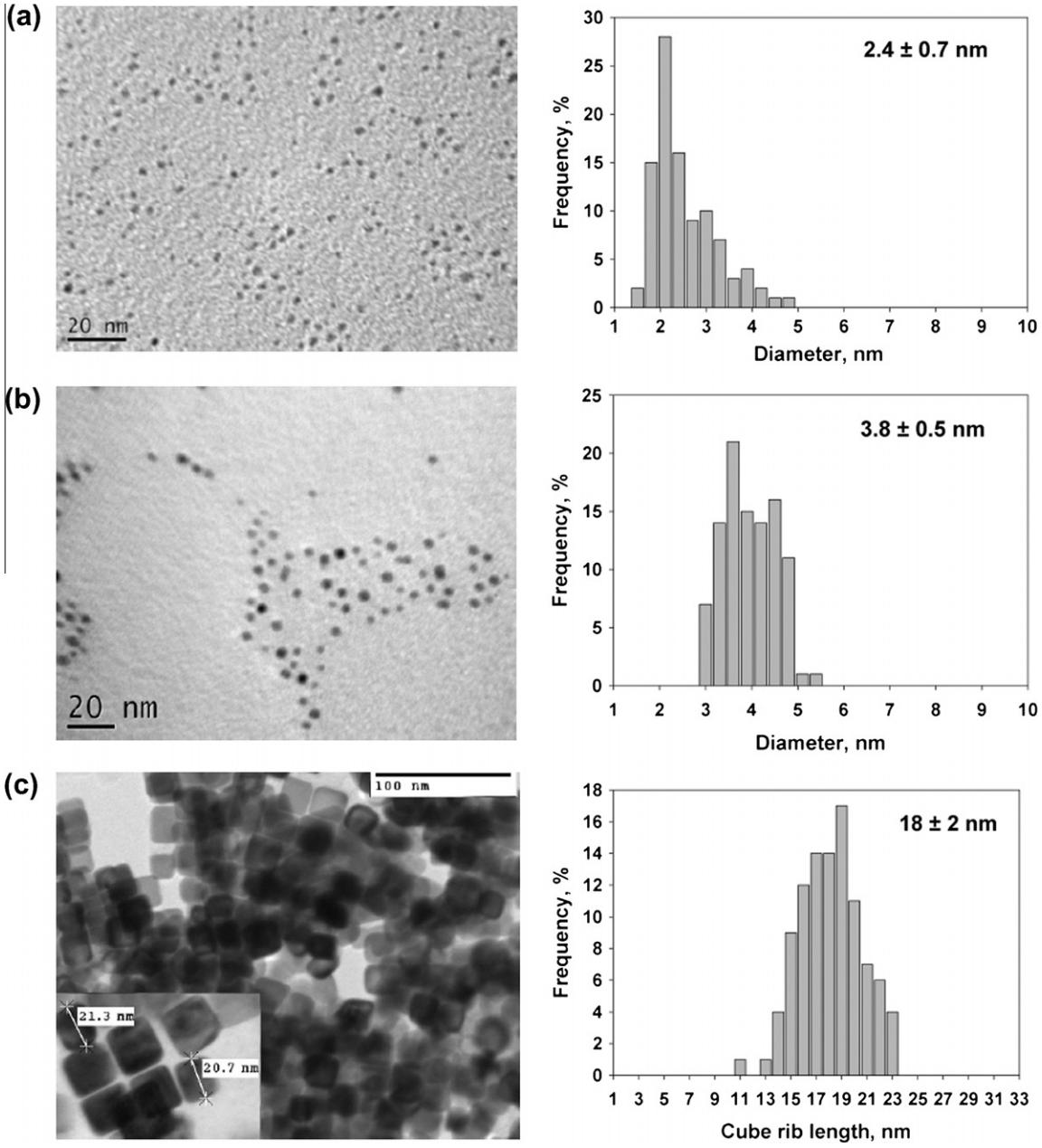

Fig. 2. TEM images and particle size distribution for Pd spheres of 2.4 and 3.8 nm diameter and Pd cubes of 18 nm rib length used in the current study.

that the plateau is not a result of catalyst poisoning with the product or the substrate.

A terminal alkyne (propargyl alcohol) may interfere with a Pd-catalyzed deallylation reaction [36], and the allyl alcohol formed as a by-product in the reaction from Fig. 1b is known to adsorb on the Pd surface for further transformations [49,50]. To verify whether the presence of allyl alcohol inhibits the reaction kinetics, several experiments were carried out with 12.5 μM substrate, 0 and 6.25 μM allyl alcohol, 56 μM Pd (2.4 nm spheres, 0.3 wt.% loading), 0.22 mol/mol substrate-to-Pd ratio, at 100 and 500 μM of PPh_3 [50]. The kinetic curves obtained from 0 to 80 min of the reactions with allyl alcohol fell within experimental errors of the curves obtained with no allyl alcohol present (similar to Fig. 3). Thus, allyl alcohol does not interfere with the catalytic reaction *via* competitive binding with the catalyst.

Kinetic curves similar to that of Fig. 3 were obtained for all tested nanostructures. As was systematically observed, product concentration increases linearly with time after a short induction period, less than 10 min, until a plateau is reached. The zero-order regions (Fig. 4) were used to estimate the reaction rates. The rates are provided in Table 1, along with turnover frequencies (TOFs) calculated per total surface atoms and specific surface atoms. If TOFs calculated per some specific atoms do not change with the particle size and/or structure, they are considered to be the reaction active sites [13,39,40,43]. Defect sites (vertex and edge atoms on Pd f.c.c. particles) were claimed to be responsible for the catalytic activity of the nanoparticles in Heck and Suzuki reactions [13,43]; thus, they were selected as probable active sites. The dispersion values, provided in Table 1, account for the loss of one plane of both Pd spheres and cubes due to the attachment to the alumina support. The details of TOF calculations may be found in the Supplementary Content. The surface statistics was determined for ideal f.c.c. cuboctahedral and cubic metal crystal as described elsewhere [5,51]. Remarkably, the turnover frequencies, calculated

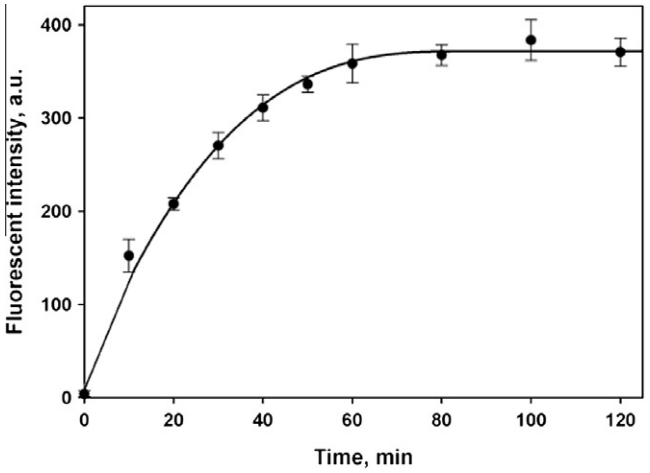

Fig. 3. Example of the kinetic curve as time-dependent fluorescence (the line is a guide for the eye), 42 μM Pd, 0.3 mol/mol substrate-to-Pd ratio, 2.4 nm Pd 0.3 wt.%/Al_2O_3, [PPh_3] = 500 μM, [ether ***1***] = 12.5 μM, 5% DMSO/pH 7 buffer solution.

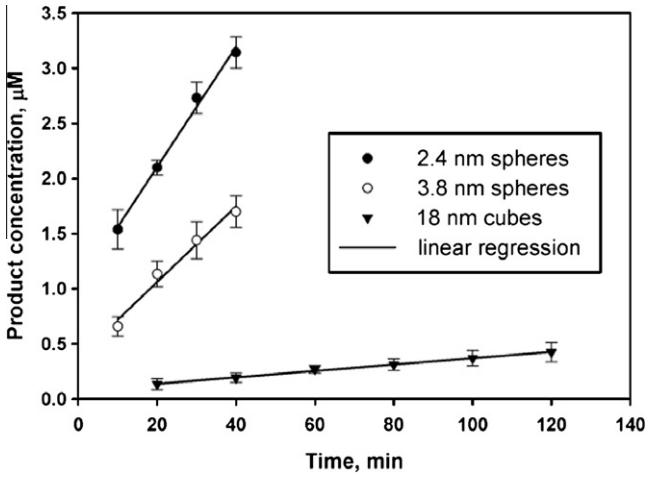

Fig. 4. Linear regions of kinetic curves used for the calculation reaction rates for 42 μM 2.4 nm Pd nanoparticles (0.5 mol/mol substrate-to-Pd ratio), 56 μM 3.8 nm Pd nanoparticles (0.22 mol/mol substrate-to-Pd ratio), and 560 μM Pd nanocubes (0.022 mol/mol substrate-to-Pd ratio); 0.3 wt.% Pd/Al_2O_3, [PPh_3] = 500 μM, [ether ***1***] = 12.5 μM, 5% DMSO/pH 7 buffer solution.

per the defect atoms, have similar values, indicating that these atoms may be active sites [13,43], even though the cubes have a different from spheres stabilizing agent (CTAB vs. PVP), which may influence the activity [52]. An important assumption for proposing defect sites as active sites for any reaction is that the nanoparticle size and shape do not change and no other active species are formed. To verify this assumption, leaching studies were conducted.

3.2. Leaching study

Leaching studies were performed for the most active 2.4-nm particles, so that the influence of reaction components, if any, is the most dramatic among the three nanoparticle samples. A 1-h reaction with 56 μM Pd, 0.22 mol/mol substrate-to-Pd ratio and 50 μM PPh_3 yielded a product concentration of 3.0 ± 0.4 μM (24% conversion). Moreover, the Pd loading on the alumina support (as determined using AAS) decreased from 0.30 ± 0.01 to 0.11 ± 0.02 wt.%. The TEM images obtained for the nanoparticles leached to the solution and left on the support (Fig. 5) show that the nanoparticle size increased from the initial 2.4 ± 0.7 to 3.2 ± 0.6 and 3.4 ± 0.6 nm, respectively, with the disappearance of smaller nanoparticles. This most likely indicates that Ostwald ripening occurs, when atoms detach from smaller nanoparticles and reattach to bigger particles, as, for example, was similarly observed in Suzuki reaction [53]. A similar size of nanoparticles after a reaction in the solution and on the support indicates that there is no preferential atom readsorption on nanoparticles in the presence of γ-Al_2O_3 due to the support effects or mass transfer limitations. In the case of 2.4-nm particles, more than 85% of surface atoms are accessible to the reactants, assuming that the particles are adsorbed through one of their (1 1 1) planes; thus, they may grow similar to the free nanoparticles during Ostwald ripening. As the experiments with only PPh_3 and the catalyst showed, PPh_3 causes nanoparticle leaching (as discussed below), while the reaction substrate is responsible for the atomic leaching of Pd atoms from low-coordinated sites on Pd nanoparticles.

The nanoparticle growth may also indicate an excess of unreduced metal ions that can deposit on nanoparticles when reduced [26]. Even though Pd(0) species are the active species in the reaction (Fig. 1), Pd^{2+} may convert to Pd^0 in the presence of PPh_3 [36], which was confirmed by ^{31}P NMR and cyclic voltammetry [54]. Indeed, when the reaction was carried out with $PdCl_2/Al_2O_3$ (56 μM Pd, 0.22 mol/mol substrate-to-Pd ratio, and 50 μM PPh_3), 2.2 μM product concentration was attained in 1 h (18% conversion). In comparison, 2.4-nm nanoparticles under the same conditions allowed 3.0 ± 0.3 μM product concentration (24% conversion). The reaction solution after 1-h reaction was analyzed by TEM, and the formation of 2.9 ± 1.1 nm nanoparticles was observed (Fig. 6). AAS of the solid catalyst after the 1-h reaction showed only 0.11 ± 0.02 wt.% Pd on Al_2O_3 vs. initial 0.3 wt.%, confirming palladium leaching to the solution. The shift in the fluorescence peak did not occur, indicating the absence of a possible Claisen rearrangement catalyzed by Pd^{2+} species [45]. Palladium and gold nanoparticle stabilization with phosphines, including PPh_3, is a known phenomenon [55,56]. *In situ* formation of Pd nanoparticles from $PdCl_2$ supported on a polymer was also found in a Suzuki reaction [57].

Table 1
Activity of Pd nanoparticles and turnover frequencies (TOF) calculated for all surface atoms and defect (edge and vertex) atoms. Calculation details are provided in Supplementary Content.

Catalyst	Rate, $10^{-2}\times$ (mol/(mol_{Pd} h))	Dispersion (all surface atoms) (%)	TOF per all surface atoms, $10^{-2}\times$ (h^{-1})	Dispersion (defect surface atoms) (%)	TOF per defect surface atoms (h^{-1})
2.4 nm spheres	5.7 ± 0.4	40	14 ± 1	13	0.43 ± 0.03
3.8 nm spheres	3.7 ± 0.4	33	11 ± 1	9	0.43 ± 0.04
18 nm cubes	0.030 ± 0.001	5	0.57 ± 0.02	0.1	0.33 ± 0.01

Reaction conditions: 56-μM Pd spheres (560-μM Pd cubes), 0.3 wt.% Pd/Al_2O_3, 0.22 mol/mol substrate-to-Pd ratio (0.022 for the cubes), [PPh_3] = 500 μM, [ether ***1***] = 12.5 μM, 5% DMSO/pH 7 buffer solution.

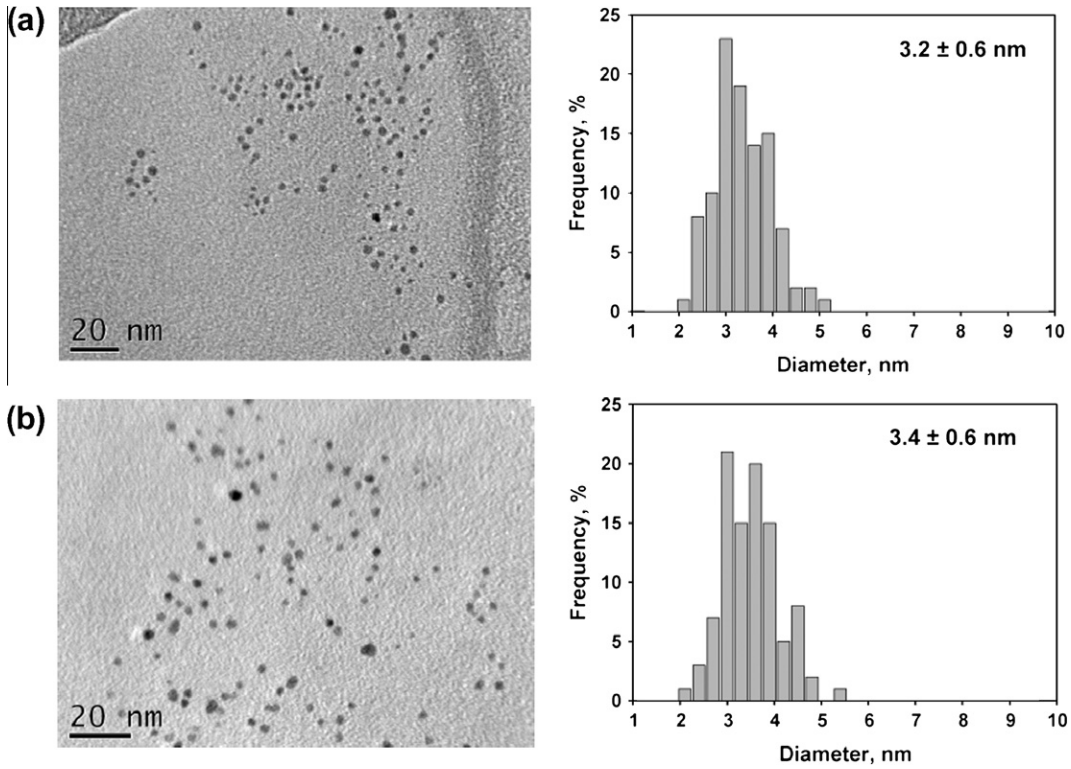

Fig. 5. Size change in Pd nanoparticles of 2.4 ± 0.7 nm (see Fig. 2a for the fresh particles) after 1-h reaction as an indication of Ostwald ripening: (a) leached to the solution; (b) remaining on the alumina support. Reaction conditions: 56 μM Pd, 0.22 mol/mol substrate-to-Pd ratio, 0.3 wt.% Pd/Al_2O_3, [PPh_3] = 50 μM, [ether ***1***] = 12.5 μM, 5% DMSO/pH 7 buffer solution.

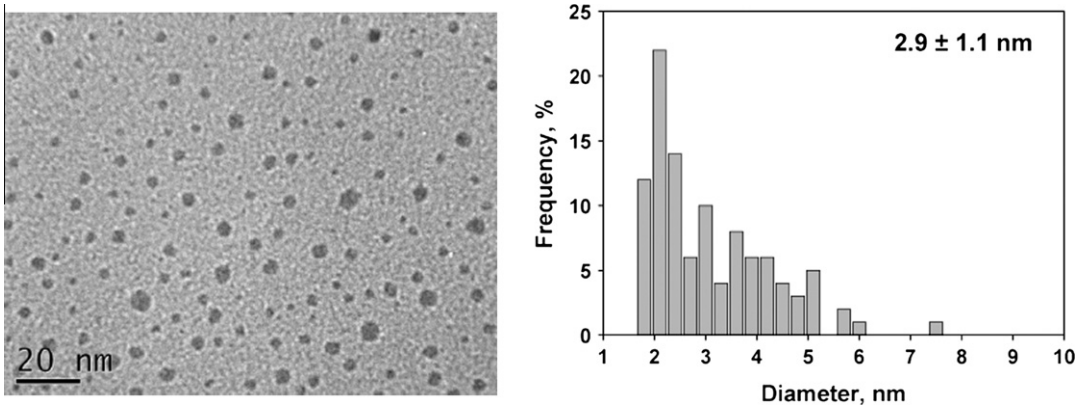

Fig. 6. Evidence of Pd(0) species formation from Pd^{2+} during the catalytic reaction: TEM image and size distribution of Pd nanoparticles formed in the solution after 1-h reaction catalyzed by $PdCl_2/Al_2O_3$, 56 μM Pd, 0.22 mol/mol substrate-to-Pd ratio, 0.3 wt.% Pd/Al_2O_3, [PPh_3] = 50 μM, [ether ***1***] = 12.5 μM, 5% DMSO/pH 7 buffer solution.

To verify whether the nanoparticle growth during a reaction with 2.4-nm nanoparticles occurs due to the Pd^{2+} reduction (as $PdCl_2$ was used as Pd precursor) and deposition on existing nanoparticles, XPS analyses of the 2.4-nm catalyst before and after 1-h reaction (50 μM PPh_3) were performed. Both samples did not show a shift in the Pd $3d_{5/2}$ characteristic peak with the binding energy of 334 eV, representative of metallic palladium. No peaks could be assigned to palladium from $PdCl_2$ or PdO (336 and 338 eV, respectively). Thus, either the reduction was complete during the nanoparticle synthesis or unreduced ions were removed during dialysis before deposition on the support. This indicates that the nanoparticle growth during the nanoparticle-catalyzed reaction did not occur through the deposition of unreduced metal ions. Furthermore, the surface carbon-to-palladium mass ratio in the fresh and used 2.4-nm catalysts, as determined from XPS, stayed approximately constant at 4.0 ± 0.3 nm, indicating that PVP did not leach from the nanoparticles, which otherwise could lead to decreased nanoparticle stabilization.

To establish which reaction mixture components played the most significant role in palladium leaching, sets of experiments with varying reaction components were performed at 0.22 mol/mol substrate-to-Pd ratio. Fig. 7a shows the fluorescence development with time for the reactions with 2.4-nm Pd nanoparticles and different PPh_3 concentrations under other equal conditions. As PPh_3 may quench fluorescence, as reported elsewhere [58], calibration curves of product fluorescence at different PPh_3 concentrations were obtained (Fig. 7b) and used to construct kinetic curves expressed as product concentration vs. time (Fig. 7c). As seen from Fig. 7c,

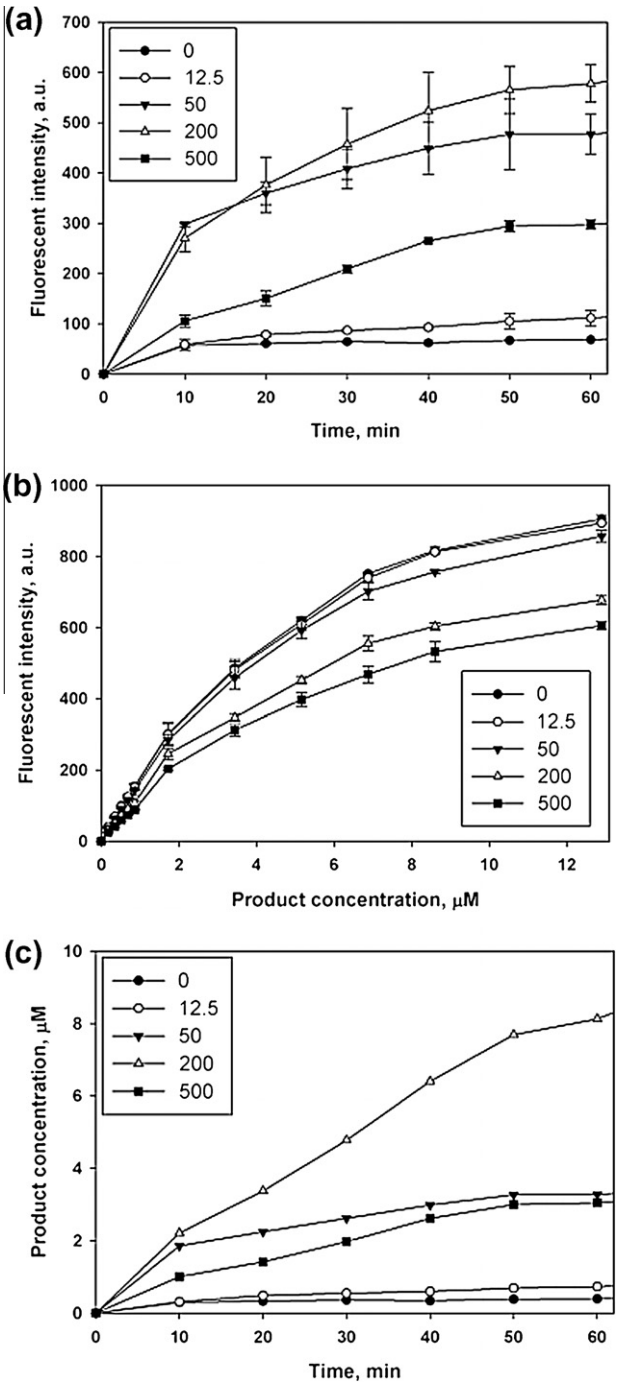

Fig. 7. Pd nanoparticle activity as a function of PPh_3 concentration: (a) influence of the PPh_3 concentration on the fluorescence development during catalytic reactions; (b) product fluorescence as seen from the calibration curves, and (c) kinetic curves expressed as product concentration vs. time. Reaction conditions: 56 μM Pd, 0.22 mol/mol substrate-to-Pd ratio, 2.4 nm Pd, 0.3 wt.% Pd/Al_2O_3, [ether ***1***] = 12.5 μM, 5% DMSO/pH 7 buffer solution. Calibration solutions: different purified product concentrations in 5% DMSO/pH 7 buffer solution at different PPh_3 concentrations.

the presence of triphenylphosphine is pivotal to the reaction, but the amount of accumulated product passes through a maximum at 200 μM of PPh_3. At this PPh_3 concentration, 100% product formation was obtained after 80 min of the reaction. Usually, triphenylphosphine is considered to be a poison of heterogeneous Pd catalysts, adsorbing on their active sites [59], which does not explain negligible reaction rates in its absence. Pd activity promotion by the addition of PPh_3 followed by a drop in activity with an increase in PPh_3 concentration was also found in nitrobenzene hydrogenation by Pd supported on nanodiamonds [60]. In a Heck reaction, addition of four equivalents of PPh_3 strongly retarded the reaction rate [18]. Suzuki reaction inhibition with the addition of PPh_3 was attributed to the phosphine competing with a substrate for ligation with Pd atom on solid surface [28]. In an allylic alkylation with Pd/C catalyst, triphenylphosphine was suggested to act as a stabilizing agent for Pd, generating a reactive Pd(0)–PPh_3 complex *in situ* [32]. A pivotal role of the presence of the triphenylphosphine was also shown during allylic substitution using heterogeneous Pd catalysts; however, the activity of heterogeneous catalysts was at least one order of magnitude lower than the activity of homogeneous $Pd(PPh_3)_4$ [37]. Pd particle size was not reported, and the trend could be attributed to the particles with low dispersions. The existence of an optimum PPh_3/Pd ratio was attributed to the formation of the most stable and active palladium clusters with the ligand, which is most likely to be the case in the current study as well. As discussed by Jones [1], high amount of added PPh_3 can deactivate potentially active leached species *via* overcoordination, which is in line with our results and the hypothesis by Koide [36] that high ligand concentration leads to the formation of less active more coordinatively saturated palladium species.

Remarkably, TEM images of 2.4-nm Pd nanoparticles found in the reaction solution in the presence of 50 μM of PPh_3 (Fig. 5a), 200 μM of PPh_3 (Fig. 8a), and 500 μM of PPh_3 (Fig. 8b) reveal that the fastest reaction with 200 μM of triphenylphosphine is concomitant with the formation of the largest particles (up to 10 nm, including multiply twinned nanoparticles), which was not observed for any other PPh_3 concentrations. Smaller particles grow into the larger ones, as, for example, Figs. 2a and 7a show that in the initial sample, ~17% of nanoparticles are smaller than 2 nm, while in the sample after the reaction, there is only 5% of such particles. The trend corresponds to the Ostwald ripening mechanism. Table 2 shows reaction rates and particle sizes for the tested catalytic systems. Palladium leaching was confirmed for the most active catalytic system with 200 μM of PPh_3: AAS measurements of Pd remaining on the support after 20, 40 and 60 min of the reaction (0.22 mol/mol substrate-to-Pd ratio) showed the Pd contents of 0.21 ± 0.02 wt.%, 0.12 ± 0.03 wt.%, 0.08 ± 0.03 wt.%, respectively, vs. 0.3 wt.% initial loading. Correlation of the leached amounts with the reaction rates between two closest data points in Fig. 7c (i.e., 0–20 min, 20–40 min, and 40–60 min) reveals that ratio of the product concentration change to the amount of the leached palladium in each time interval is 0.19 ± 0.02 μM product/wt.% Pd leached, which again confirms that the reaction occurs *via* Pd leaching. Apparently, the reaction requires that Pd atoms leach from Pd nanoparticles, forming active species with triphenylphosphine (as there is no reaction without the ligand), and redeposit on the nanoparticles leading to their growth. Higher PPh_3 concentration likely leads to the improved nanoparticle stabilization upon re-deposition and formation of less-active catalytic species, as discussed above. XPS analysis of a used Pd(2.4 nm)/Al_2O_3 catalyst showed the presence of phosphorus on the catalyst surface at the P/Pd atomic ratio of 10. The PPh_3 presence influences not only the atomic leaching but also the formation of the most active catalytic species.

To verify whether the active species formation depends on the origin of palladium species, in addition to the $PdCl_2$-catalyzed reaction discussed above in this Section, the reactions with two homogeneous complexes $Pd(PPh_3)_4$ and $PdCl_2(PPh_3)_2$ were carried at different PPh_3 concentrations (Table 3) at 0.5 mol/mol substrate-to-Pd ratio. $Pd(PPh_3)_4$ complex shows the activity increase with the ligand concentration increase from 200 to 500 μM, which reflects the trend in the dramatic nanoparticle activity increase with the ligand concentration increase from 0 to 200 μM (Fig. 7c and Table 2). However, the reaction rate with $Pd(PPh_3)_4$ catalyst at 500 μM

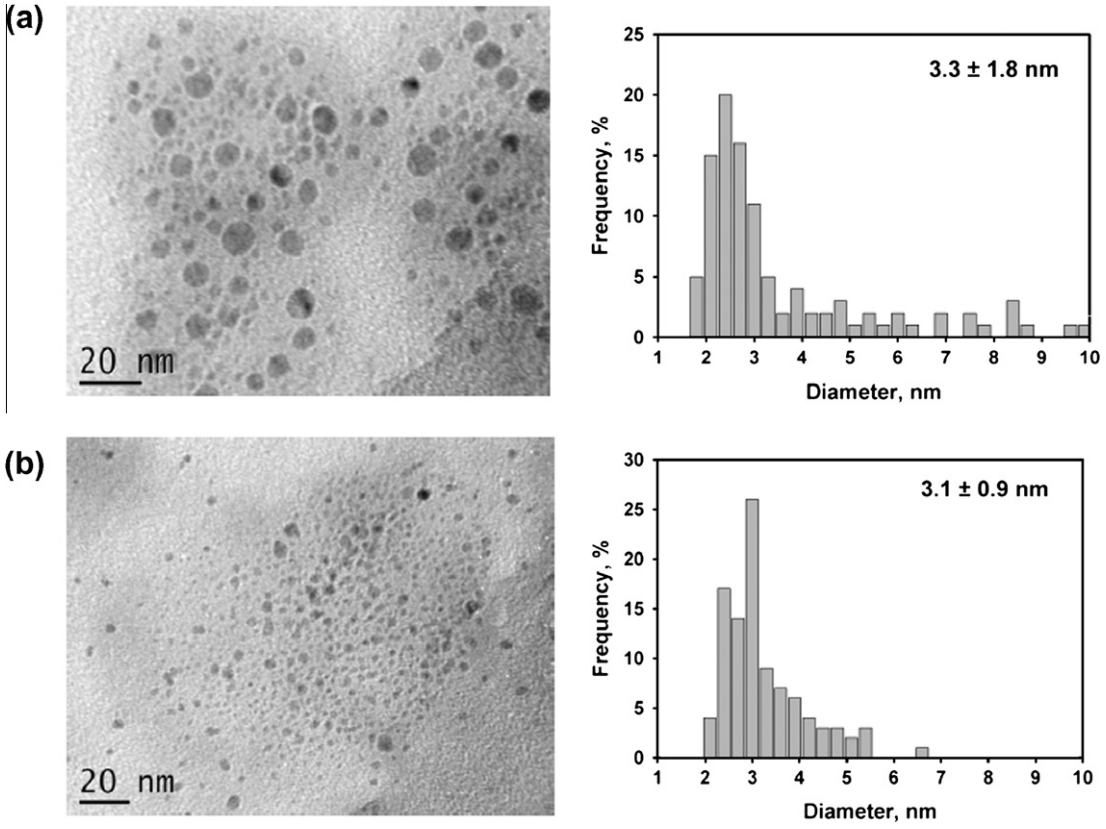

Fig. 8. Size of Pd nanoparticles in the reaction solutions as a function of PPh_3 concentration: TEM images and size distribution for 2.4 nm Pd nanoparticles found in the solutions after 1 h of the catalytic reactions (56 μM Pd, 0.22 mol/mol substrate-to-Pd ratio, 0.3 wt.% Pd/Al_2O_3, [ether ***1***] = 12.5 μM, 5% DMSO/pH 7 buffer): (a) with 200 μM PPh_3 and (b) with 500 μM PPh_3. Compare with the fresh catalyst (Fig. 2a) and the catalyst after the reaction with 50 μM PPh_3 (Fig. 5a).

Table 2
Catalytic activity and nanoparticle size as a function of PPh_3 concentration.

[PPh_3] (μM)	[PPh_3]/[total Pd] (mol/mol)	[PPh_3]/[surface Pd] (mol/mol)	Rate, 10^{-2} (mol/(mol_{Pd} h))	Nanoparticles in the reaction solution after 1-h reaction (nm)
2.4-nm Pd spheres, 56 μM Pd, 0.3 wt.%/Al_2O_3				
0	0	0	0.18 ± 0.09	–
12.5	0.2	0.6	0.98 ± 0.21	–
50	1	2	4.1 ± 0.02	3.2 ± 0.6
200	4	9	15.0 ± 0.7	3.3 ± 1.8
500	9	22	5.7 ± 0.4	3.1 ± 0.9
Homogeneous catalyst, 25 μM $Pd(PPh_3)_4$				
500	24	24	3.4 ± 0.1	2.8 ± 0.5

Reaction conditions: [ether ***1***] = 12.5 μM, 0.22 mol/mol substrate-to-Pd ratio (0.5 for the homogeneous catalyst), 5% DMSO/pH 7 buffer solution, 1-h reaction. "–" means no data are available.

Table 3
Catalytic activity of homogeneous Pd complexes.

Pd complex	[PPh_3] (μM)	[PPh_3]/[Pd] (mol/mol)	Product concentration after 1-h reaction (μM)	Nanoparticles in the reaction solution after 1-h reaction (nm)
$Pd(PPh_3)_4$	200	12	0.77 ± 0.03	–
$Pd(PPh_3)_4$	500	24	1.30 ± 0.02	2.8 ± 0.5
$PdCl_2(PPh_3)_2$	0	2	1.40 ± 0.01	3.0 ± 0.7
$PdCl_2(PPh_3)_2$	500	22	0.47 ± 0.01	2.7 ± 0.8

Reaction conditions: 25 μM Pd complex, 0.5 mol/mol substrate-to-Pd ratio, [ether ***1***] = 12.5 μM, 5% DMSO/pH 7 buffer solution, 1 h reaction. "–" means no data are available.

PPh_3 concentration is $(3.4 \pm 0.1) \times 10^{-2}$ mol/(mol_{Pd} h), which is 1.7-fold lower per mole of total Pd as compared to the 2.4-nm particles and 4-fold lower as compared to the amount of surface Pd atoms (Table 2). Pd nanoparticles were found after a 1-h reaction carried out with $Pd(PPh_3)_4$ (Table 3). The nanoparticles were also found after a 1-h reaction catalyzed by $PdCl_2(PPh_3)_2$, even in the absence of PPh_3. It is known that the complex is able to undergo reduction to Pd(0) in the presence of hydroxide anion [61]; Claisen rearrangement of the reaction substrate catalyzed by Pd^{2+} was not observed as the fluorescence peak did not shift. The complex shows similar activity to other homogeneous catalysts, and its activity decreases when 500 μM PPh_3 is added. The trend of decreasing activity with increasing ligand concentration is concomitant with the trend observed for 2.4 nm Pd nanoparticles, when their activity decreases as the ligand concentration was increased from 200 to 500 μM (Fig. 7c and Table 2). Most likely, in this case, high ligand concentration leads to the formation of less-active more coordinatively saturated palladium species as proposed by Koide [36]. Comparing [PPh_3]/[Pd] ratios and corresponding activities from Tables 2 and 3, one can see that not only the values, but also the trends are different for Pd nanoparticles, $Pd(PPh_3)_4$, and $PdCl_2(PPh_3)_2$. Selection of a proper palladium precursor for the *in situ* formation of Pd nanoparticles active in C–C coupling reactions is known to have a very important effect on the structure and catalytic activity of the nanoparticles [57]. Thus, the presence of PPh_3 in the coordination sphere of Pd(0) is a necessary condition for the reaction to occur, but the optimum [PPh_3]/[Pd] ratio depends on the origin of Pd atoms, with the most active ones among the catalytic systems studied being the surface atoms of 2.4-nm Pd nanoparticles. As discussed in Section 3.1, defect sites

are the potential sources of active Pd species, most likely due to their lowest coordination number. The nature of the active catalytic species is not addressed in the present study and should be explored further.

Even though Pd atomic leaching and re-deposition are PPh_3 dependent, the question remains as to whether the ligand is solely responsible for the atomic dissolution. Two control experiments with 2.4-nm catalyst (0.3 wt.% Pd/Al_2O_3, 56 μM, 0.22 mol/mol substrate-to-Pd ratio, 5% DMSO/pH 7 buffer) were carried out with 0 and 200 μM PPh_3 concentrations, without the addition of the reaction substrate (ether ***1***). After 1 h of stirring, the catalyst was removed by centrifugation and analyzed using AAS for Pd loading, and solutions were analyzed using TEM. When no substrate and no PPh_3 were present, 0.3 wt.% Pd loading on the catalyst was found, indicating that leaching does not occur in the absence of the catalytic reaction. When 200 μM PPh_3 was present without the substrate, 0.23 wt.% Pd loading was found on the support, but the solution contained nanoparticles of the same size as the fresh catalyst (2.5 ± 0.8 nm vs. fresh 2.4 ± 0.7 nm). The value of 0.23 wt.% is higher than the value of 0.08 wt.% obtained after 1-h reaction with 200 μM PPh_3, 0.56 μM Pd, 0.22 mol/mol substrate-to-Pd ratio, indicating again the leaching is more profound *in situ*, when the reaction substrate is present, as compared to the nanoparticle leaching caused by only PPh_3. Apparently, the presence of triphenylphosphine contributes to the nanoparticle leaching, but the presence of ether ***1*** is pivotal to the atomic leaching (Fig. 8a). Atomic dissolution due to the oxidative addition of a reactant was proposed earlier for the Sonogashira reaction [21] and is confirmed in the current study for the fluorometric Tsuji–Trost reaction. As the turnover frequencies were correlated with the amount of defect (edge and vertex) atoms on the nanoparticle surface, leaching of low-coordinated atoms on Pd surface is likely to occur, which was proposed for a Sonogashira reaction [20].

As Ostwald ripening was found to happen only in the presence of ether ***1*** and is PPh_3-concentration dependent, the ether ***1*** is proposed to bind to low-coordinated Pd^0 atoms on smaller Pd particles and cause atomic leaching. Pd nanoparticles, thus, serve as a reservoir of catalytically active species. Active species formation is PPh_3 dependent; there is no reaction in the absence of phosphine, and the reaction rate passes through maximum as PPh_3 concentration increases. The further drop in activity as the PPh_3 concentration increases is most likely due to the existing equilibrium between highly coordinated Pd species and lower-coordinated species co-existing with the free ligand. More coordinatively saturated palladium species were also proposed by Koide as less active in the homogeneously catalyzed reaction [36]. After a catalytic cycle, Pd atoms redeposit on the remaining nanoparticles, leading to their growth. The proposed mechanism and observations should be considered in light of the studied reaction (Fig. 1b), and more reaction substrates should be tested before a general conclusion on Tsuji–Trost catalysis by Pd nanoparticles could be drawn.

4. Conclusions

A Tsuji–Trost reaction for the conversion of non-fluorescent ether ***1*** to fluorescent phenol ***2*** (Fig. 1b) was successfully performed using Pd nanospheres of 2.4 and 3.8 nm diameter and Pd nanocubes of 18 nm rib length. The catalytic activity was correlated with the amount of defect (edge and vertex) atoms on the different nanoparticle surfaces. However, TEM and AAS analyses, combined with kinetic studies in the presence of different reaction mixture components, showed that the reaction occurs through the atomic dissolution *via* the oxidative addition of ether ***1***, probably to the defect sites on the nanoparticles. Furthermore, 2.4-nm nanoparticles were found to be most active at the molar ratio of PPh_3/Pd of 4 in the range from 0 to 9, leading to the formation of nanoparticles of up to 10 nm diameter, including multiply twinned particles. The absence of triphenylphosphine was detrimental to the reaction, but high ligand concentration also led to lower catalytic activity. Homogeneous $Pd(PPh_3)_4$ catalyst was found to be less active than the 2.4-nm Pd nanoparticles, indicating the formation of other homogeneous active species in the nanoparticle-catalyzed reaction. More detailed studies on the formed homogeneous active species should follow, especially for a variety of substrates, but this study, for the first time, demonstrates the validity of the atomic dissolution mechanism in the Pd nanoparticle-catalyzed fluorometric Tsuji–Trost reaction (Fig. 1b).

Acknowledgments

We thank MicroSystems Technology Research Initiative (MSTRI) at the University of Alberta for financial support, Dr. Dimitre Karpuzov (Alberta Centre for Surface Engineering and Science, University of Alberta) for XPS analysis, and Allen Reule for the help with TOF calculations.

Appendix A. Supplementary material

Supplementary data associated with this article can be found, in the online version, at doi:10.1016/j.jcat.2011.04.009.

References

[1] N.T.S. Phan, M.V.D. Sluys, C.W. Jones, Adv. Synth. Catal. 348 (2006) 609.
[2] R. Narayanan, M.A. El-Sayed, J. Phys. Chem. B 109 (2005) 12663.
[3] D. Astruc, Inorg. Chem. 46 (2007) 1884.
[4] M. Lamblin, L. Nassar-Hardy, J.-C. Hierso, E. Fouquet, F.-X. Felpin, Adv. Synth. Catal. 352 (2010) 33.
[5] N. Semagina, L. Kiwi-Minsker, Catal. Rev. 51 (2009) 147.
[6] D. Astruc, Tetrahedron: Asymmetry 21 (2010) 1040.
[7] D. Astruc, Molecules 15 (2010) 4947.
[8] D. Astruc, F. Lu, J.R. Aranzaes, Angew. Chem. Int. Ed. 44 (2005) 7852.
[9] A. Biffis, M. Zecca, M. Basato, J. Mol. Catal. A 173 (2001) 249.
[10] L. Huang, P.K. Wong, Curr. Org. Synth. 7 (2010) 599.
[11] B. Karimi, H. Behzadnia, E. Farhangi, E. Jafari, A. Zamani, Curr. Org. Synth. 7 (20110) 543.
[12] J. Guerra, M.A. Herrero, Nanoscale 2 (2010) 1390.
[13] J. Le Bars, U. Specht, J.S. Bradley, D.G. Blackmond, Langmuir 15 (1999) 7621.
[14] A.V. Gaikwad, A. Holuigue, M.B. Thathagar, J.E. teh Elshof, G. Rothenberg, Chem. – Eur. J. 13 (2007) 6908.
[15] M. Dieguez, O. Pamies, Y. Mata, E. Teuma, M. Gomez, F. Ribaudo, P.W.N.M. van Leeuwen, Adv. Synth. Catal. 350 (2008) 2583.
[16] C.C. Cassol, A.P. Umpierre, G. Machado, S.I. Wolke, J. Dupont, J. Am. Chem. Soc. 127 (2005) 3298.
[17] J.G. de Vries, Dalton Trans. (2006) 421.
[18] M. Beller, H. Fischer, K. Kuhlein, C.P. Reisinger, W.A. Herrmann, J. Organomet. Chem. 520 (1996) 257.
[19] R.L. Augustine, S.T. O'Leary, J. Mol. Catal. 7 (1992) 229.
[20] M.B. Thathagar, P.J. Kooyman, R. Boerleider, E. Jansen, C.J. Elsevier, G. Rothenberg, Adv. Synth. Catal. 347 (2005) 1965.
[21] M.B. Thathagar, J.E.T. Elshof, G. Rothenberg, Angew. Chem. Int. Ed. 45 (2006) 2886.
[22] L. Chen, S. Hong, X. Zhou, Z. Zhou, H. Hou, Catal. Commun. 9 (2008) 2221.
[23] S. Gao, N. Zhao, M. Shu, S. Che, Appl. Catal. A 388 (2010) 196.
[24] C. Duplais, A.J. Forman, B.A. Baker, B.H. Lipshutz, Chem. – Eur. J. 16 (2009) 3366.
[25] A.K. Diallo, C. Ornelas, L. Salmon, J.R. Aranzaes, D. Astruc, Angew. Chem. Int. Ed. 46 (2007) 8644.
[26] R. Narayanan, K. Tabor, M.A. El-Sayed, Top. Catal. 48 (2008) 60.
[27] P.J. Ellis, I.J.S. Fairlamb, S.F.J. Hackett, K. Wilson, A.F. Lee, Angew. Chem. Int. Ed. 49 (2010) 1820.
[28] S.P. Andrews, A.F. Stepan, H. Tanaka, S.V. Ley, M.D. Smith, Adv. Synth. Catal. 347 (2005) 647.
[29] G. Budroni, A. Corma, H. Garcia, A. Primo, J. Catal. 251 (2007) 345.
[30] F. Lu, J. Ruiz, D. Astruc, Tetrahedron Lett. 45 (2004) 9443.
[31] C.R. LeBlond, A.T. Andrews, Y. Sun, J.R.J. Sowa, Org. Lett. 3 (2001) 1555.
[32] F.-X. Felpin, Y. Landais, J. Org. Chem. 70 (2005) 6441.
[33] T. Mitsudome, K. Nose, K. Mori, T. Mizugaki, K. Ebitani, K. Jitsukawa, K. Kaneda, Angew. Chem. Int. Ed. 46 (2007) 3288.
[34] S. Jansat, M. Gomez, K. Philippot, G. Muller, E. Guiu, C. Claver, S. Castillon, B. Chaudret, J. Am. Chem. Soc. 126 (2004) 1592.
[35] F. Song, A.L. Garner, K. Koide, J. Am. Chem. Soc. 129 (2007) 12354.
[36] A.L. Garner, F. Song, K. Koide, J. Am. Chem. Soc. 131 (2009) 5163.
[37] D.E. Bergbreiter, B. Chen, J. Chem. Soc., Chem. Commun. (1983) 1238.

[38] I. Favier, M. Gomez, G. Muller, M.R. Axet, S. Castillon, C. Claver, S. Jansat, B. Chaudret, K. Philippot, Adv. Synth. Catal. 349 (2007) 2459.
[39] R. Ma, N. Semagina, J. Phys. Chem. C 114 (2010) 15417.
[40] N. Semagina, A. Renken, D. Laub, L. Kiwi-Minsker, J. Catal. 246 (2007) 308.
[41] B.A. Sparano, S.P. Shahi, K. Koide, Org. Lett. 6 (2004) 1947.
[42] T. Teranishi, M. Miyake, Chem. Mater. 10 (1998) 594.
[43] Y. Li, E. Boone, M.A. El-Sayed, Langmuir 18 (2002) 4921.
[44] W. Niu, Z.-Y. Li, L. Shi, X. Liu, H. Li, S. Han, J. Chen, G. Xu, Crystal Growth Design 8 (2008) 4440.
[45] A.L. Garner, K. Koide, J. Am. Chem. Soc. 130 (2008) 16472.
[46] Y. Xiong, Y. Xia, Adv. Mater. 19 (2007) 3385.
[47] F. Baletto, R. Ferrando, Rev. Mod. Phys. 77 (2005) 371.
[48] M.A. Vannice, Kinetics of Catalytic Reactions, Springer, New York, 2005.
[49] O.M. Wilson, M.R. Knecht, J.C. Garcia-Martinez, R.M. Crooks, J. Am. Chem. Soc. 128 (2006) 4510.
[50] S. Bhattacharjee, D.M. Dotzauer, M.L. Bruening, J. Am. Chem. Soc. 131 (2009) 3601.
[51] R. Van Hardeveld, F. Hartog, Surf. Sci. 15 (1969) 189.
[52] R. Narayanan, M.A. El-Sayed, J. Phys. Chem. B 108 (2004) 8572.
[53] R. Narayanan, M.A. El-Sayed, J. Am. Chem. Soc. 125 (2003) 8340.
[54] C. Amatore, A. Jutand, M.A. M'Barki, Organometallics 11 (1992) 3009.
[55] M. Tamura, H. Fujihara, J. Am. Chem. Soc. 125 (2003) 15742.
[56] Y. Yanagimoto, Y. Negishi, H. Fujihara, T. Tsukuda, J. Phys. Chem. B 110 (2006) 11611.
[57] T. Borkowski, A.M. Trzeciak, W. Bukowski, A. Bukowska, W. Tylus, L. Kepinski, Appl. Catal. A 378 (2010) 83.
[58] S. Takagi, T. Okamoto, T. Shiragami, H. Inou, J. Org. Chem. 59 (1994) 7373.
[59] S. Siegel, J.A. Hawkins, J. Org. Chem. 51 (1986) 1638.
[60] I.I. Obraztsova, N.K. Eremenko, Y.N. Velyakina, Kinet. Catal. 49 (2008) 401.
[61] V.V. Grushin, H. Alper, Organometallics 12 (1993) 1890.